2016 IEEE International Conference on Robotics and Automation (ICRA)
Stockholm, Sweden, May 16-21, 2016

A continuous jumping robot on water mimicking water striders*

Jihong Yan, *Member, IEEE*, Kai Yang, Tao Wang, Xinbin Zhang and Jie Zhao, *Member, IEEE*

***Abstract*—Aiming at mimicking the jumping locomotion of water striders, a new continuous jumping robot on water is proposed. Compared with the horizontal rowing motion, the jumping capability of water striders is challengeable to imitate, since the impact force on water is easy to cause the sinking of the robot. In this paper, a jumping mechanism based on springs is designed to produce a large thrust for the robot to jump. The shape of supporting legs and center of gravity of the robot are carefully designed so that the robot can jump on the surface continuously and smoothly. Influences of several critical factors, including the area of supporting legs, spring stiffness and jumping angle, on jump performance are analyzed by means of dynamic simulation and experiments. The fabricated robot weighs about 10.2 g and can continuously jump on water with the maximum leap height and length of 120 mm and 410 mm, respectively.**

I. Introduction

In recent years, the high-efficient and agile water-surface locomotion of water striders has attracted substantial interests of researchers [1]-[5]. At present, the research on water strider robots is mainly focused on mimicking its skating movement. Till now, A numerous of robots that can skate on water have been designed using superhydrophobic materials as supporting legs and actuating legs [6]-[10]. For example, Sitti et al. [8] designed a miniature water strider robot driven by a T-shaped actuating mechanism with three piezoelectric actuators. Yan et al. [10] proposed a novel cam-link mechanism that can generate an ellipse-like spatial trajectory and ensure the actuating legs row on water without penetrating into water during the rowing stage.

Imitating the jumping locomotion of water striders has proved to be a severe technical challenges. Since the legs are easy to pierce the surface if they press the surface with a large force, result in the sinking of the robot [11], [12]. Besides, in order to jump continuously, reasonable configuration of the gravity is also essential to ensure the robot contact with the water surface with an optimal posture, so that the robot can always maintain a stable state. Zhao et al. [13] designed the first water-jumping robot driven by springs. Yan et al. [14] proposed a new water jumping robot actuated by two DC motors, simple force analysis and simulation research were carried out to optimize its structure. Recently, Je-sung Koh et.al [15] designed a water jumping robot based on the sheet SMA Actuator, it jumps as high on water as it can on land and its maximum jumping height can reach 142mm, showing an amazing jumping performance. However, the robot can only achieve a single hop and its load capacity is too small to carry out some aquatic tasks.

In this paper, a new continuous jumping robot on water was designed. We first introduce the structure design of the robot in section II. Then the force models for supporting legs and actuating legs are established in section III. In order to clarify the jumping performance of the robot, the influencing factors, including the position of the gravity, jumping angle, the area of supporting legs and the speed of the actuating legs were studied by dynamics simulation in section IV. Based on the above analysis, the robot is fabricated and a series of experiments were conducted to verify the effects of these factors on jumping performance in section V.

II. Structure Design

A. Jumping Mechanism

Fig.1 shows the jumping mechanism of the robot. The actuating legs are driven by a micro DC motor through a set of reduction gears and incomplete gears. In one working period, the DC motor drives the incomplete gears mechanism and propels the two actuating legs swing forward, the springs are tensioned to store elastic potential. When the incomplete gears rotate to a certain angle, the actuating legs are released, the elastic potential stored by the springs actuates the legs hitting the water surface rapidly. The reaction force drives the body jumping out of water surface. The DC motor rotates continuously, so that the robot can jump continuously. The direction the actuating legs hitting the water surface can be conveniently adjusted by changing the jumping angle (ε) between the swing base and base.

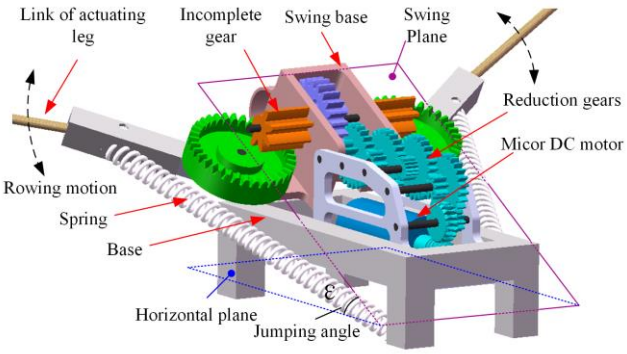

Figure 1. Jumping mechanism of the robot

*Research supported by Natural Science Foundation of China (NSFC, Grant 51305098).

Jihong Yan is with State Key laboratory of Robotics and Systems, Harbin Institute of Technology, Harbin 150001, P. R. China (corresponding author to provide phone: 86-451-86413392; fax: 86-451-86413392; e-mail: jhyan@hit.edu.cn).

Kai Yang, Tao Wang and Xinbin Zhang is with State Key laboratory of Robotics and Systems, Harbin Institute of Technology, Harbin 150001, P. R. China

Jie Zhao is with State Key laboratory of Robotics and Systems, Harbin Institute of Technology, Harbin 150001, P. R. China

B. Design of Supporting Legs

For a water-jumping robot, its legs can easily penetrate into the water surface when detaching from and falling back into the water surface, which may lead to the sinking of the robot. So it's necessary to choose a reasonable shape of the legs to achieve stable and continuous jumping process.

Fig.2 illustrates the failure conditions and supporting forces of cylindrical and rectangular legs. As shown in the figure, the changing of the position of the three-phase contact lines (P_c) with the depth are different, leading to different failure conditions.

For a cylindrical leg, the three-phase contact lines rise along the circumference, as shown by the red dotted line. When the distance between the air-water interface and three-phase contact line (d_1) is bigger than the distance between the center of the cylinder and three-phase contact line (d_2), the air-water interface of the two sides will contact resulting in the sinking of the leg. For a rectangular leg, the three-phase contact line rise along the two sides from P_{c0} to P_c and then is trapped at P_c until the failure condition is triggered. If the width of the rectangle (W) is large, the menisci of the two sides can hardly contact with each other, the leg will not sink into the water unless the angle θ measured from the horizontal direction to the tangential direction of the liquid surface at the triple point increases to the contact angle of the material θ_c.

The figure also shows the supporting forces, which can be divided into three parts: the buoyancy generated by the volume of the leg (the red area), the buoyancy caused by hydrophobicity (the green area) and surface tension (the purple area). Assuming that there are no complex water surface behaviors at the ends of the legs, then the supporting force can be calculated.

For a cylindrical leg, when given the submerged angle β and contact angle θ_c of the material, the supporting force can be calculated:

$$F_s = \rho g l[-2Rh_0 \sin\beta + \beta R^2 - R^2 \sin\beta\cos\beta] + 2\gamma(l + 2R\cos\beta)\sin\varphi \quad (1)$$

Where l and R are the length and diameter of the leg. γ is the surface tension coefficient of water, h and h_0 is the height from the leg's bottom and three-phase contact line to the water surface respectively. In this paper, the height is defined negative when a leg falls into water.

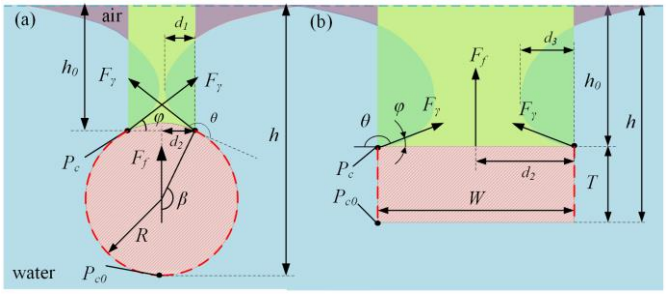

Figure 2. Faliure conditions and supporting forces of cylindrical and rectangular legs

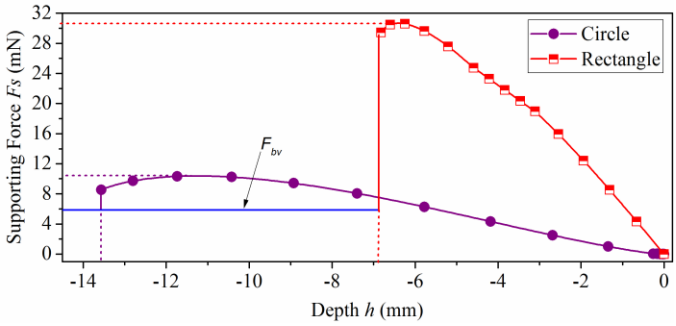

Figure 3. Changing of the supporting forces exerted on the supporting leg

For a rectangular leg, according to the mathematical model of the air-water interface [13], when given the depth of the leg, the supporting force can be calculated:

$$F_s = -\rho g l W h + 2\gamma(l + W)\sin\varphi \quad (2)$$

According to (1) and (2), the changing of the supporting forces exerted on cylindrical and rectangular legs with the same cross-section area (60mm^2) are shown in figure 3. The character length and contact angle of the legs are 10mm and 160° respectively. At this time, the width (W) and thick (T) of the rectangle is 40mm and 1.5mm.

As shown in the figure, the maximum supporting force caused by a rectangular leg is more than 2.5 times bigger than a cylindrical leg. Since the volume of the legs are the same, the buoyancy forces caused by the volume of the two legs (F_{bv}) are the same, as shown by the horizontal solid line. The buoyancy force caused by hydrophobicity plays an important role on the supporting force.

Unlike the buoyancy generated by the submerged object, the buoyancy caused by hydrophobicity is mainly influenced by the surface area and hydrophobicity of the material, the drag force when the floating material moves along the surface is far less than a submerged object. Although a rectangular leg with a big surface area may decrease the effect of surface tension on supporting force, it can bring a large supporting force and small drag force, which is necessary for the a water-jumping robot. So rectangle is chosen as the cross section of the legs.

III. Force Modelling

The forces exerted on a rectangular leg, including buoyance force (F_b), surface tension (F_γ), hydrodynamic pressure (F_d) and viscous force (F_μ), play an important role on the jumping movement and stability, as shown in fig.4.

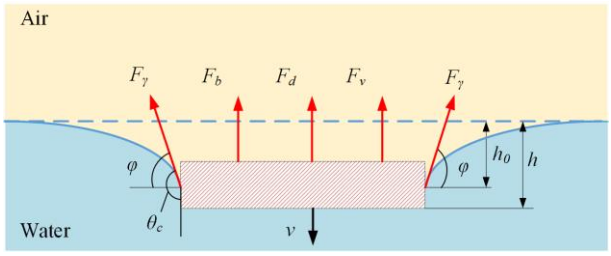

Figure 4. Forces exerted on a rectangular leg when falling on the water surface

The total supporting force can be written as:

$$F_s = -\rho_{water} ghs + \gamma l \sin\varphi + \frac{1}{2} c \rho_{water} s v^2 \quad (3)$$

Where, the viscous force F_μ is considered in the hydrodynamic pressure by a correction coefficient c to simplify the calculation [14].

A. Supporting force on water surface

When the robot floats on the water surface, the hydrodynamic force F_d can be ignored since the velocity of the legs is small. At this time, the supporting force F_s can be calculated by (4).

$$F_S = -\rho_{water} gsh + \gamma l \sin\varphi \quad (4)$$

Since rectangle is chosen as the cross-section of the legs, it's necessary to clarify the influence of its dimension on buoyancy force and surface tension. Fig.5 shows the influence of the leg's width on supporting force and the ratio of buoyance and surface tension. The width of the legs changes from 1.5 mm to 5.0 mm when the thickness and length remain unchanged at 1.5 mm and 10 mm respectively. In the figure, F1.5, F5.0 are the supporting forces when the width is 1.5 and 5.0mm. P1.5, P5.0 are the ratio of total buoyancy force (F_b) and surface tension (F_γ) when the width is 1.5 mm and 5.0 mm respectively.

The results reveal that an increase in width (W) and depth (h) of the rectangle results in a large supporting force (F_s) and ratio of buoyancy force (F_b) and surface tension (F_γ), indicating that the contribution of surface tension (F_γ) to supporting force decreases with the increase of the width.

B. Detaching from the water surface

Fig.6 illustrates the forces exerted on a supporting leg when it detaches from the water surface. The total force F_s can be described by (5).

$$F_s = \rho_{water} gsh + \gamma l_c \sin\varphi + \frac{1}{2} c \rho_{air} s v^2 \quad (5)$$

According to (5), when the supporting leg detaches from the water surface with a certain speed, the hydrodynamic force F_d remains unchanged. At this time, with the increase of the material's contact angle, the maximum leaving height h_{max} and the angle φ (φ=180°-θ) decreases, leading to the decrease of the vertical component of surface tension. So hydrophobic legs with higher contact angle are preferred to decrease the drag force in the jumping process.

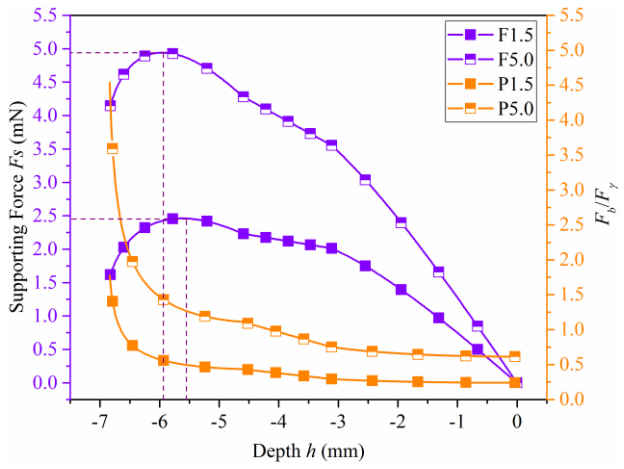

Figure 5. Influence of leg's width on the supporting force and ratio of F_b and F_γ

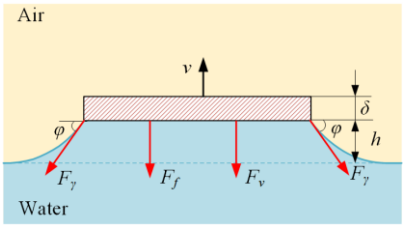

Figure 6. Forces exerted on a supporting leg when leaving the water surface

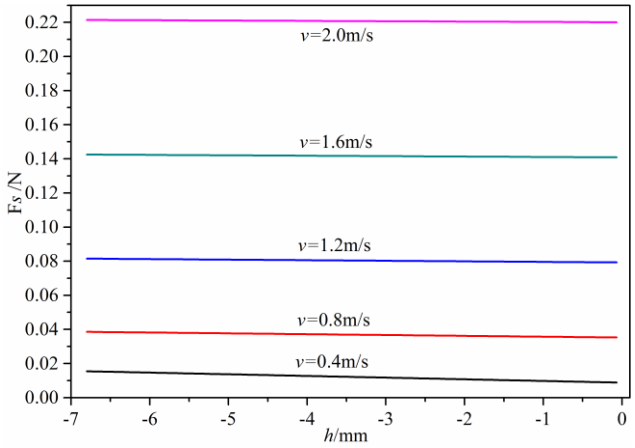

Figure 7. Changing of the supporting force with the speed and falling depth

C. Falling back to the water surface

When the robot falls back to the water surface with a large speed, the hydrodynamic force F_d plays a main role on the supporting force, the surface tension can be ignored. The supporting force mainly consists of hydrodynamic force and hydrostatic force. Fig.7 illustrates the changing of supporting force with the falling speed and depth, the dimension of the leg is 10 mm long, 10 mm wide and 1.5 mm thick. The supporting force changes slowly with the depth at a certain speed, the curve is approximately a horizontal line, indicating that the buoyancy force accounts for a smaller proportion in the total supporting force. At a certain depth, the supporting force increases rapidly with the increase of the leg's speed, illustrating that the hydrodynamic force play a main function.

D. Forces Exerted on the Actuating Legs

For an actuating leg, its velocity is usually large during the jumping process, so the hydrodynamic force plays an important role, as shown in fig.8. In this case, the surface tension can be ignored, the actuating force can be divided into a horizontal component and a vertical component:

$$F_A = \begin{cases} \frac{1}{2} c \rho_\Delta s v^2 \cos\alpha - \rho g \Delta h s \\ \frac{1}{2} c \rho_\Delta s v^2 \sin\alpha - \rho g h_c s \end{cases} \quad (6)$$

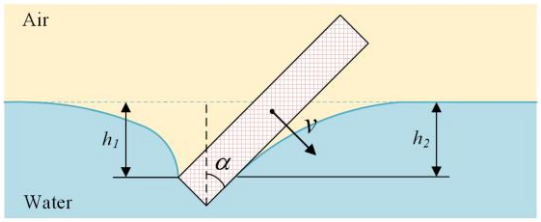

Figure 8. Forces exerted on an actuating leg when falling into the water

where F_A is the total force applied on the actuating legs, α is the angle between the vertical plane and the leg; $\Delta h=h_2-h_1$ is the depth difference of the air-water interface of the two sides, h_c is the equivalent depth of the actuating leg.

IV. Dynamic Analysis

A. Simulation Model

In order to clarify the robot's jumping performance, the jumping process is simulated based on ADAMS by changing the position of the center of gravity, area of the supporting legs, jumping angle and the stiffness of the spring.

Fig.9 shows the simulation model. The actual forces exerted on the legs are uniformly distributed. Restricted by the software, in the model, each leg is divided into four or six grids on which the forces are exerted, including the vertical force F_{vij}, the horizontal force F_{hij} and the torque in the jumping plane M_{hij}. Where i represents the number of the leg, j is the number of the grid. According to section III, the surface tension can be ignored since it plays a limited role in the jumping process, then F_{vij}, F_{hij} and M_{hij} satisfy (7).

$$\begin{cases} F_{vij}=\int_{S_{ij}}\rho g h_{ij}dS_{ij}+\frac{1}{2}\int_{S_{ij}}c_{vij}\rho v_{vij}{}^2dS_{ij} \\ F_{hij}=\frac{1}{2}\int_{S_{ij}}c_{hij}\rho v_{hij}{}^2dS_{ij} \\ M_{ij}=\int_{S_{ij}}\rho g h_{ij}(\vec{v_k}\times\vec{r_k})dS_{ij}+\frac{1}{2}\int_{S_{ij}}c_{kij}\rho v_{kij}{}^2(\vec{v_k}\times\vec{r_k})dS_{ij} \end{cases} \tag{7}$$

Where $\vec{v_k}$ is a unit vector, $\vec{r_k}$ is the displacement between the center of gravity and the center of a grid. Then the jumping movement of the robot can be described by (8).

$$\begin{cases} ma=\sum(F_{vij}+F_{hij})-mg \\ I\alpha=\sum M_{ij}+\sum(F_{vij}+F_{hij})\times\overrightarrow{\chi_k} \end{cases} \tag{8}$$

Where a and α are the acceleration and angle acceleration at the center of gravity respectively, I is the moment of inertia, $\overrightarrow{\chi_k}$ is the displacement between the center of the gird and the center of the gravity of the robot.

The jumping properties of the robot are analyzed by ADAMS and compared with experimental results in the section V.

B. Center of Gravity Position

The effect of the gravity configuration on jumping posture is stimulated by adjusting the center of gravity, as shown in fig.10. When the actuating legs strike the water surface, if the center of gravity is above the swing plane, there will exist a torque promoting the robot to fall backward and even overturn, which is not conducive to the continuously jumping of the robot. When the center of gravity is below the swing plane, the torque reverses, the jumping posture changes from falling backwards to leaning forwards, making the jumping process stable. So G_3 is chosen as the robot's center of gravity. In this case, the front supporting leg will touch the water first. In order to further improve the impact resistance of the robot, a single front leg is used, its shape is designed as a trapezoid and the front end of the leg is curled to reduce the force per unit area, so that the robot can fall back on the water surface smoothly instead of penetrating into the water.

V. Results and Discussion

The new water-jumping robot was fabricated, as shown in fig.11. In order to reduce the robot's weight, the body and reduction mechanism were made by 3D printing technique. The supporting legs and actuating legs were made of hydrophobic nickel foam with a contact angle of 143° and a thickness of 1.5 mm. The initial area of the front supporting leg, rear supporting legs and actuating legs are 4000 mm^2, 1900 mm^2 and 1400 mm^2 respectively.

In order to clarify the jumping performance, experiments were conducted by changing the area of supporting legs, spring stiffness and jumping angle.

A. Influence of the Supporting Legs' area

The forces exerted on the supporting legs directly influence

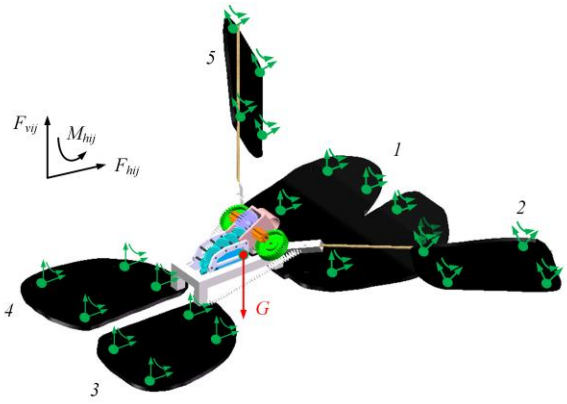

Figure 9. Illustration of the simulation model

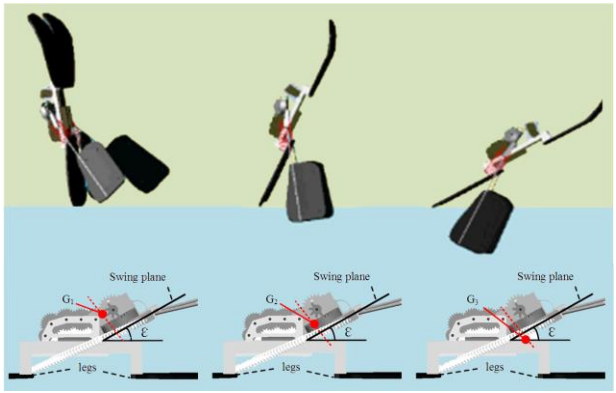

Figure 10. Influence of gravity center on jumping posture

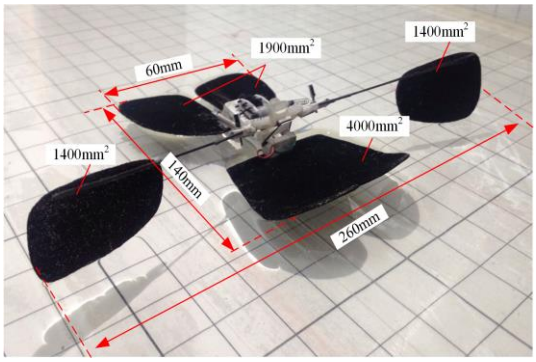

Figure 11. Photogrtaph of the fabricated water-jumping robot

the jumping performance. A larger area leads to stronger supporting force. However it will increase the drag force (F_s) at the same time. So the impact of the area of legs is simulated and analyzed by keeping the shape of the supporting legs unchanged and adjusting the area from 0.5 to 1.5 times of the initial area, the results are shown in fig.12.

The simulation and experiments show that, with the decrease of the legs' area, the jumping height and distance increase, resulting in a better jumping performance. The experiments also demonstrate that the robot is easy to sink into the water when the area is too small, since the force exerted on per unit area of the legs increase, endangering its precarious state at the surface and causing it to sink. Under the condition of sufficient supporting force, legs with small area are preferred. Taking into account of the performance and stability, the 0.75 times of the initial area of legs was chosen for the subsequent experiments.

B. Influence of the Springs' stiffness

If the actuating legs hit the water surface with a big velocity, the hydrophobicity of the legs decreases, the drag force will become dominant, which will affect the jumping performance. On the contrary, the robot can't detach from the water surface at a low speed. The influence of the stiffness of springs on jumping performance is shown in fig.13. Considering the output torque of the motor, the stiffness in the experiments was set as 0.08, 0.09 and 0.10 N/mm respectively.

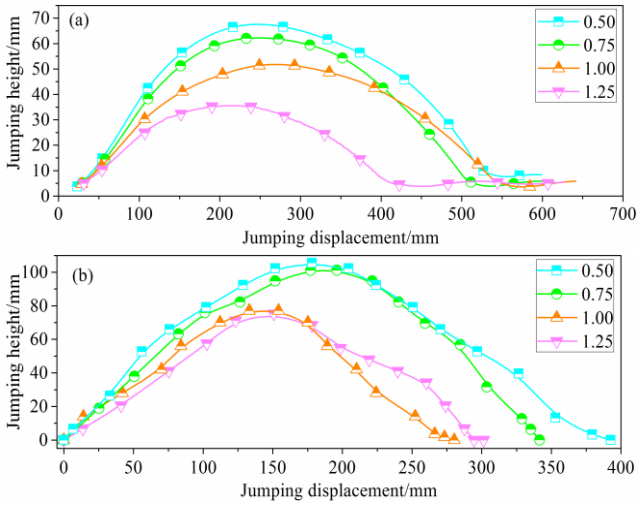

Figure 12. Change of jumping trajectory with the total area of supporting legs: (a) simulation and (b) experiment

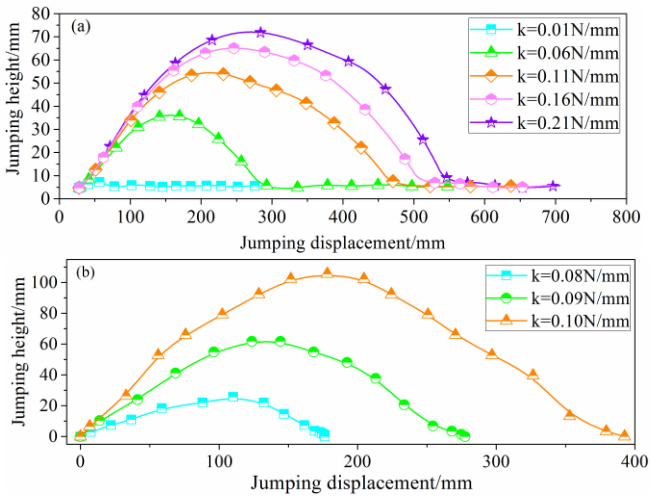

Figure 13. Change of jumping trajectory with the stiffness of the springs: (a) simulation and (b) experiment

Both the simulation and experiment show that, the jumping height and distance increase with the increase of the stiffness. The simulation result also illustrates that the jumping height and distance increase slowly when the stiffness is bigger than 0.10N/mm. Since the further increase of the stiffness will accelerate the wear of the drive mechanism, 0.10 N/mm is chosen as the ideal spring stiffness.

C. Influence of the Jumping Angle

The influence of jumping angle on jumping posture and performance is also stimulated and tested, as shown in fig.14. The simulation result shows that the jumping displacement and height increase with the increase of the jumping angle. The experiments show that the jumping displacement and height increases gradually when the jumping angle increases from 10° to 25°. When the angle is bigger than 30°, the robot's jumping height reaches a peak and fluctuates with a small amplitude, while the displacement significantly reduces. This is because the actuating force in the horizontal direction decreases fast. When the angle reaches 40°, the robot sinks into the water due to its unreasonable jumping posture. So, the jumping angle is set to 25°.

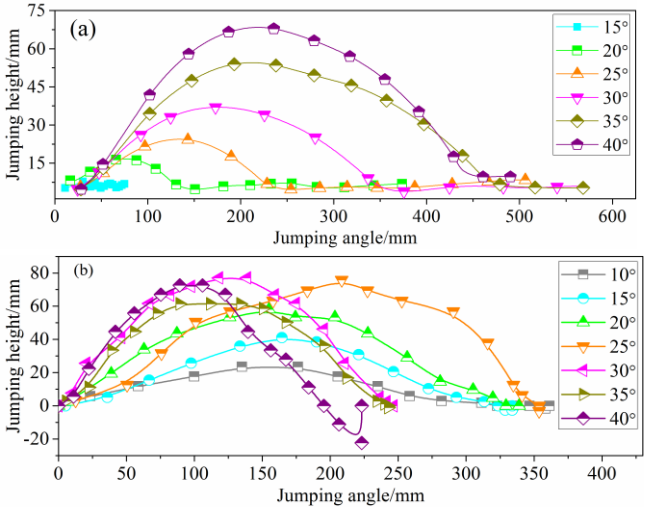

Figure 14. Change of jumping trajectory with the jumping angle: (a) simulation and (b) experiment

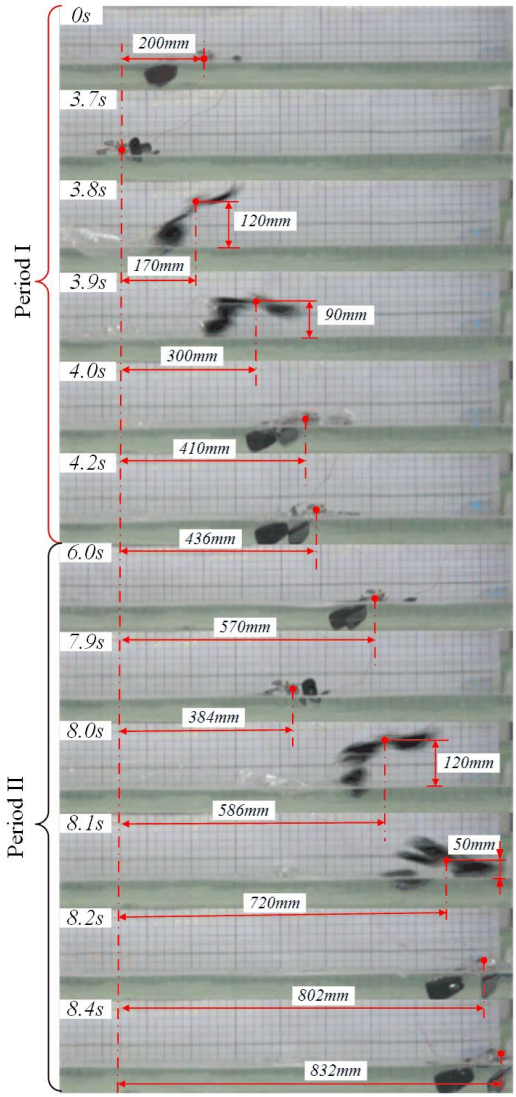

Figure 15. Snapshot of the robot jumping on the water surface continously

From the above simulation and experimental results, we can see that under the same parameters, the actual jumping height is usually greater than that of the simulation, while the actuating jumping displacement is smaller. There are two possible reasons responsible for the error between the simulation and experimental results: on one hand, the force models constructed in section III need further improvement. On the other hand, there exists some difference between the simulation model and the actual robot. In the simulation model, the legs are divided into grids to exert the forces due to the limitation of the software simulation environment, while the actual forces exerted on the legs are uniformly distributed and changed continuously with the falling depth.

D. Continuous Jumping

Based on the above simulation and experimental results, the optimal parameters are determined. The area of front supporting leg and rear supporting legs are 3000 mm^2 and 1500 mm^2 respectively. The area of the actuating legs is set to 1000 mm^2. The stiffness of springs and the jumping angle are 0.10 N/mm and 25°. The length of the robot is about 140 mm. Fig.15 shows the continuous jumping process of the robot. In a typical jump, the robot can jump 120 mm high and 410 mm long with a jumping period of 4.2 s.

VI. Conclusion

A new continuous jumping robot on water was proposed. Jumping mechanism based on springs was proposed to provide large impulsive forces for the jumping motion. The effect of the structure parameters of the robot on jumping performance was analyzed by simulations and experiments. The fabricated robot weighs about 10.2 g and can jump on water continuously with a maximum leap height and length of 120 mm and 410 mm respectively. The robot makes full use of the buoyance caused by hydrophobicity. Despite the fact that the surface tension plays a limited role in the jumping movement, the robot still shows a notable agility and jumping performance. The robot can be easily equipped with some devices to carry out various aquatic tasks due to its big load capacity.

References

[1] D. L. Hu, B. Chan, and J. W. M. Bush, "The hydrodynamics of water strider locomotion," *Nature*, vol. 424, pp. 663-666, 2003.

[2] M. W. Denny, "Paradox lost: answers and questions about walking on water," *Journal of experimental biology*, vol. 207, pp. 1601-1606, 2004.

[3] X. Gao and L. Jiang, "Biophysics: water-repellent legs of water striders," *Nature*, vol. 432, pp. 36-36, 2004.

[4] X.-Q. Feng, X. Gao, Z. Wu, L. Jiang, and Q.-S. Zheng, "Superior Water Repellency of Water Strider Legs with Hierarchical Structures: Experiments and Analysis," *Langmuir*, vol. 23, pp. 4892-4896, 2007/04/01 2007.

[5] T. Yabe, K. Chinda, and T. Hiraishi, "Computation of surface tension and contact angle and its application to water strider," *Computers & fluids*, vol. 36, pp. 184-190, 2007.

[6] D. L. Hu, M. Prakash, B. Chan, and J. W. Bush, "Water-walking devices," *Experiments in Fluids*, vol. 43, pp. 769-778, 2007.

[7] O. Ozcan, H. Wang, J. D. Taylor, and M. Sitti, "STRIDE II: A Water Strider-inspired Miniature Robot with Circular Footpads," *International Journal of Advanced Robotic Systems*, vol. 11, 2014.

[8] Y. S. Song and M. Sitti, "Surface-tension-driven biologically inspired water strider robots: Theory and experiments," *IEEE Transactions on Robotics*, vol. 23, pp. 578-589, 2007.

[9] X. B. Zhang, J. Zhao, Q. Zhu, N. Chen, M. Zhang, and Q. Pan, "Bioinspired Aquatic Microrobot Capable of Walking on Water Surface Like a Water Strider," *ACS Applied Materials & Interfaces*, vol. 3, pp. 2630-2636, 2011/07/27 2011.

[10] X. B. Zhang, J. H. Yan, J. Zhao, G. F. Liu, H.G. Cai, and Q. M. Pan, "A miniature surface tension-driven robot mimicking the water-surface locomotion of water strider," *IEEE International Conference on Robotics and Automation*, pp. 3172-3177, 2015.

[11] J. W. M. Bush and D. L. Hu, "Walking on water: Biolocomotion at the interface," in *Annual Review of Fluid Mechanics*. vol. 38, ed Palo Alto: Annual Reviews, 2006, pp. 339-369.

[12] D. L. Hu and J. W. Bush, "The hydrodynamics of water-walking arthropods," *Journal of Fluid Mechanics*, vol. 644, pp. 5-33, 2010.

[13] J. Zhao, X. Zhang, N. Chen, and Q. Pan, "Why Superhydrophobicity Is Crucial for a Water-Jumping Microrobot? Experimental and Theoretical Investigations," *ACS applied materials & interfaces*, vol. 4, pp. 3706-3711, 2012.

[14] J. Yan, T. Wang, X. Zhang, and J. Zhao, "Structural design and dynamic analysis of biologically inspired water-jumping robot," in *IEEE International Conference on Information and Automation*, pp. 1295-1299, 2014.

[15] J.-S. Koh, E. Yang, G.-P. Jung, S.-P. Jung, J. H. Son, S.-I. Lee, et al., "Jumping on water: Surface tension–dominated jumping of water striders and robotic insects," *Science*, vol. 349, pp. 517-521, July 31, 2015.